LA-UR-18-28501
Approved for public release; distribution is unlimited.

Title: Field Demonstration of the Combined Use of Thermally-Degrading and Cation-Exchanging Tracers to Predict Thermal Drawdown in a Geothermal Reservoir

Author(s): Reimus, Paul William
Caporuscio, Florie Andre
Marina, Oana C.
Janney, David

Intended for: Report

Issued: 2018-09-06

# Field Demonstration of the Combined Use of Thermally-Degrading and Cation-Exchanging Tracers to Predict Thermal Drawdown in a Geothermal Reservoir

Paul Reimus[1], , Florie Caporuscio[1], and Oana Marina[1] and David Janney[2]
[1]Los Alamos National Laboratory and [2]Cyrq Energy, Inc.
Prepared for the U.S. Department of Energy Geothermal Technologies Office

## Abstract

This paper presents the results and interpretation of a reactive tracer test in a geothermal reservoir involving a cation-exchanging tracer to interrogate flow pathway surface area to volume ratios and a thermally-degrading tracer to interrogate average flow pathway temperatures. The test interpretations, which are based on comparing the reactive tracer responses to that of a nonreactive tracer, are used to predict when thermal drawdown will occur at the production well due to injecting cooler, spent geothermal water into an injection well. It is shown that the cation-exchanging tracer provides constraints on the timing of thermal drawdown, and the thermally-degrading tracer provides constraints on the magnitude of thermal drawdown. Thus, the combined use of the two reactive tracers provides a better prediction of thermal drawdown than either one alone. Uncertainties associated with the method, including assumptions made about flow pathway geometry, are discussed. It is also shown that interrogating average temperatures along flow pathways using a thermally-degrading tracer *at different times* can be translated into an estimate of when thermal drawdown will occur without direct knowledge of flow pathway geometry.

## 1. Introduction

Rapid water travel times between injection and production wells in geothermal reservoirs are considered detrimental to geothermal power plant performance because they can result in rapid cooling of production well temperatures (i.e., thermal drawdown), which can decrease power generating efficiency. Water travel times between wells are typically determined by analyzing "breakthrough curves" (concentration vs. time or concentration vs. volume) of nonreactive tracers at production wells. If a rapid tracer breakthrough is observed, the corresponding injection well is usually shut-in to avoid thermal drawdown at the production well. However, in some cases it may be possible to continue to use pathogenic injection wells for some time before thermal drawdown occurs, which would buy time for installation of new injection wells without experiencing a reduction in injection capacity. Alternatively, if the predicted eventual magnitude of thermal drawdown is minimal, it might make sense to simply accept the limited drawdown and continue to operate at a slightly reduced generating efficiency rather than invest in a new injection well.

The timing and magnitude of thermal drawdown are dependent not only on the water travel time (or, more specifically, the water residence time distribution) between an injection and production well, but also on the heat transfer properties and average temperatures of the flow pathways between the wells. Nonreactive tracers provide little or no information on these characteristics. For two flow pathways of equal water residence time, the pathway with the larger surface area to volume ratio (where surface area is the interfacial area between rock and

water) will typically have a shorter thermal drawdown time because heat is transferred more efficiently from hot rock to cool water when surface area to volume ratios are larger. Average flow pathway temperatures, by themselves, do not affect the timing of thermal drawdown, but they affect its magnitude. Thus, estimates of surface area to volume ratios and average temperatures in flow pathways are complimentary and can be used to provide estimates of both timing and magnitude of thermal drawdown.

Average flow pathway temperatures in a reservoir can be interrogated using a thermally-degrading tracer that does not otherwise react in the reservoir, and the interrogation of surface area to volume ratios in flow pathways can, in principle, be accomplished using a tracer that adsorbs reversibly to rock surfaces along the flow path . The theory behind the use of these tracers for such purposes is discussed Sections 4.2 and 4.4, respectively, of Williams et al. (2013). In both cases, the interrogations are based on comparing the responses of the reactive tracer with that of a nonreactive tracer that is injected simultaneously with the reactive tracer. Additional discussion of the use of thermally-degrading tracers is provided in Plummer et al. (2011), who successfully used thermally-degrading tracers in a geothermal reservoir at Raft River, ID. Additional information on the use of cation-exchanging tracers as a special case of adsorbing tracers is provided in Dean et al. (2015) and Reimus et al. (2018).

In this paper, we present the results and interpretation of a tracer test in a geothermal reservoir involving a cation-exchanging tracer to interrogate flow pathway surface area to volume ratios and a thermally-degrading tracer to interrogate average flow pathway temperatures. Both tracers were injected simultaneously with a nonreactive tracer. The test was conducted in the fall of 2017 at the Lightning Dock Geothermal HI-01, LLC (LDG) facility located southwest of Lordsburg, NM (Figure 1) between an injection well and a production well that are herein designated as wells I and P, respectively[1]. Detailed information about the geology of the site can be found in Elston et al. (1983), Lawton and Clemons (1992), and Lawton (2000). It was known from a nonreactive tracer test conducted in 2016 that there was a very short inter-well water residence time (about 2.5 days for first tracer arrival and about a week for peak concentrations) between wells I and P (Reimus et al., 2016). Almost as soon as this short residence time became apparent, injection of cool water (from which heat had been extracted for power generation) into well I was decreased and then stopped completely as a precaution to avoid thermal drawdown at well P. Figure 2 shows a stratigraphic cross-section of the two wells, including the locations of the well screens or open intervals in each well. The wells are approximately 800 feet apart at the surface, although it is apparent that the inter-well flow pathways must involve significant vertical downward flow as well as horizontal flow. The 2017 test was conducted to gather more information on the heat transfer characteristics and average temperatures of the rapid flow pathways, thus allowing more informed estimates of how long it might take for thermal drawdown to occur at well P and the magnitude of eventual thermal drawdown as a result of the injecting cool water into well I.

To our knowledge, the 2017 LDG tracer test represents the first time that a thermally-degrading tracer has been used in conjunction with an adsorbing tracer to interrogate reservoir flow pathway characteristics. The objective of this paper is to show how this combination of two reactive tracers can provide better information for the prediction of thermal drawdown than

[1] The operator of the LDG facility requested that the well identities not be revealed, but the identities are not important for the stated objectives of this paper.

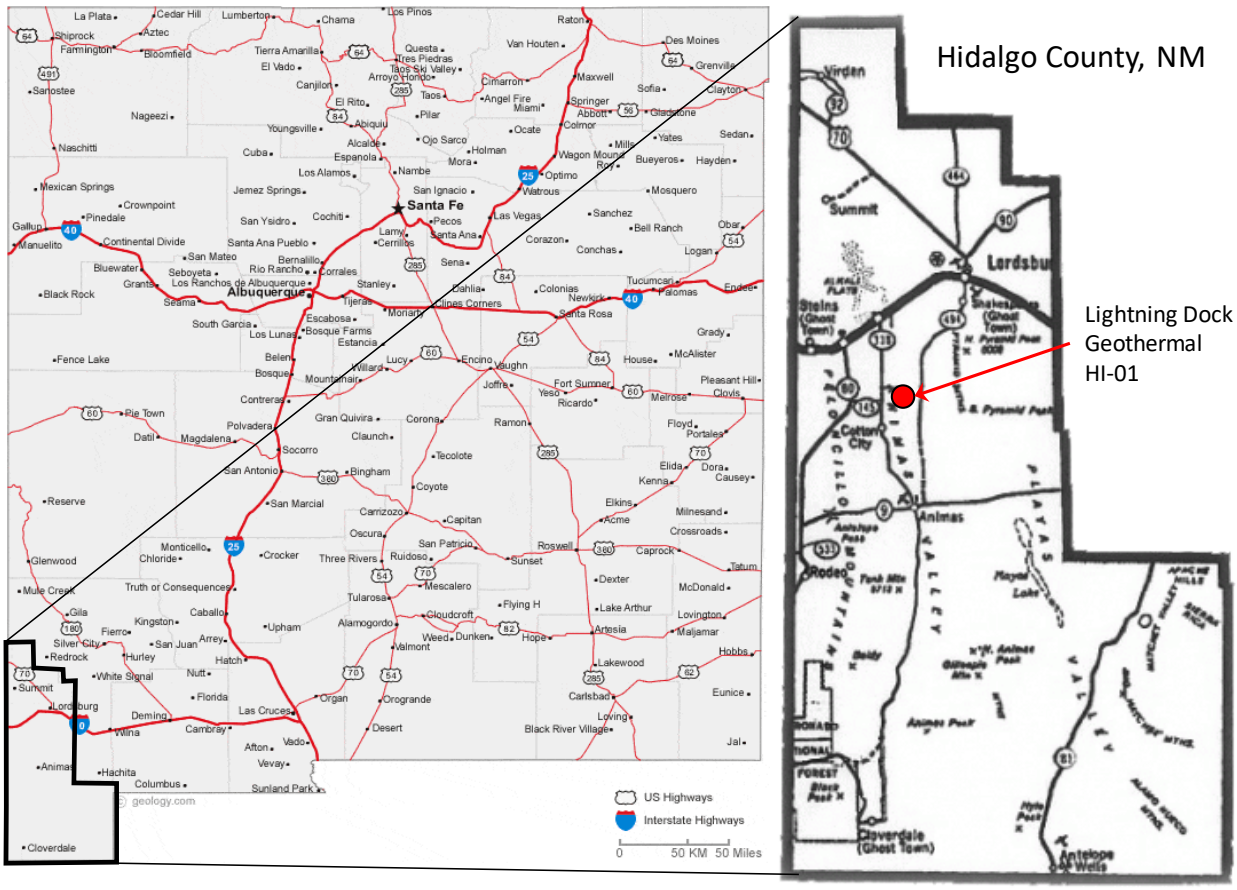


**Figure 1.** Location of the Lightning Dock Geothermal HI-01, LLC (LDG) site.

either tracer alone. However, we also discuss uncertainties and limitations of the combined use of the reactive tracers, as well as some ways that these uncertainties might be reduced.

## 2. Materials and Methods

### *2.1 Reactive Tracer Properties*

To properly use reactive tracers to estimate reservoir heat transfer properties, it is necessary to accurately describe their reactive transport behavior in the reservoir. The two reactive tracers used in the 2017 LDG tracer test were cesium ion ($Cs^+$), an adsorbing tracer that interacts by cation exchange with fracture surfaces and butyramide, a thermally-degrading tracer that has reasonably well known degradation rates as a function of temperature. $Cs^+$ was selected as the adsorbing tracer because it has relatively low background concentrations in the LDG reservoir (much lower than the other cation tracer considered, lithium ion), and also because it is not subject to thermal decay, which could affect many other candidate adsorbing tracers (e.g., dyes or other organic compounds) at the elevated reservoir temperatures. Reasons for selection of butyramide as the thermally decaying tracer are discussed later in this section. The test also involved the simultaneous injection of a nonreactive tracer (1,5-naphthalene disulfonate, or 1,5-

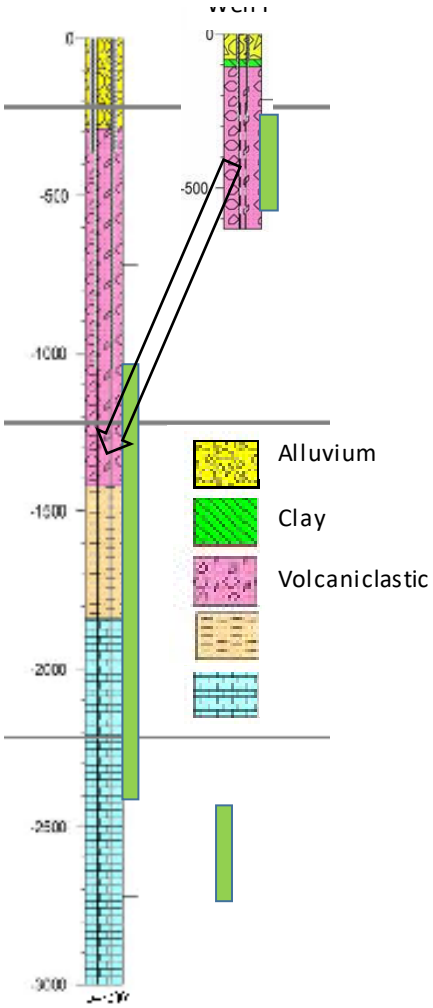


**Figure 2.** Well completions of wells P and I, and the lithologies in each well. Arrow indicates tracer transport direction in the tracer test. Depths are in feet. Wells are located approximately 800 feet apart at the surface.

NDS) with the reactive tracers, which allowed the responses of the reactive tracers to be interpreted by comparing them to the response of the nonreactive tracer.

For $Cs^+$, the equilibrium partition coefficient for adsorption onto reservoir rock surfaces (ml/g) is needed for test interpretation. Los Alamos National Laboratory (LANL) conducted laboratory experiments at elevated temperatures in rocking gold bag autoclave reactors to measure $Cs^+$ adsorption on two of the three lithologies penetrated by well P. The experiments were conducted using approximately a 10:1 mass ratio of geothermal water collected from one of the LDG production wells to cuttings from two different LDG injection wells. The cuttings from one injection well were taken from 410 ft below ground surface (bgs) and were representative of the volcaniclastics in which the injection interval in well I is completed (Fig. 2). The cuttings taken from the other injection well were about a 50:50 mass mix from 1900-1910 and 1950-1960

ft bgs and were considered representative of a siltstone that underlies the volcaniclastics. The flow pathways between wells I and P likely fall within these two lithologies, although the volcaniclastics are logically the more dominant lithology because this is the only lithology in the well I injection interval, and it is also the uppermost lithology in well P, closest to the bottom of well I (Fig. 2). Limestone samples representative of the bottom of the production interval in well P were not tested because of the less likely transport of tracers through this deeper lithology and because limestone tends to have a lower cation exchange capacity than the other types of rocks.

The resulting $Cs^+$ partition coefficients as a function of temperature in the two experiments with the different rock types are shown in Figure 3. The experiments were conducted by equilibrating the geothermal water spiked with ~12 mg/L $Cs^+$ with the rocks for two days each at successive temperatures of 25ºC, ~100ºC, ~150 C, ~100ºC, and 25ºC (i.e., a temperature cycle beginning and ending at 25ºC and cycling through reservoir temperatures). It is apparent that $Cs^+$ adsorption decreases with temperature, consistent with the observations of Dean et al. (2015), and the adsorption is somewhat greater with the siltstone than with the volcaniclastics. Also, hysteretic effects do not appear to be large at reservoir temperatures (100ºC or greater).

For butyramide, it is necessary to know the first-order (or pseudo first-order) thermal decay rate constant ($hr^{-1}$) to infer flow pathway temperatures from the tracer response (Section 4.2 of Williams et al., 2013). A decay rate constant for butyramide was not measured experimentally in this study, but rather it was deduced from the thermal decay rate constants obtained experimentally by Robinson and Tester (1990). The second order rate constants reported by Robinson and Tester (1990) were obtained at much higher temperatures (ranging from 170ºC to 238ºC) than those at LDG, so they were extrapolated to lower temperatures using an Arrhenius plot of ln($k$) vs. 1/T, where $k$ is the rate constant, and T is the temperature in degrees Kelvin. Figure 4 shows the Robinson and Tester data (at temperatures less than 210ºC) plotted in this manner with a linear regression fit to the data. This fit was used to predict rate constants at 100ºC, 125ºC and 150ºC, which should span the range of temperatures that might be encountered between wells I and P given that well P produces water at around 120ºC and the water injected into well I during the tracer test was ~100ºC.

The second-order rate constant of Robinson and Tester (1990) applies to the following rate expression for the hydrolysis reaction that causes butyramide degradation:

$$\frac{dC}{dt} = -k[OH^-]C \qquad (1)$$

where, $C$ = concentration of butyramide, mol/L
$[OH^-]$ = concentration of hydroxide ion, mol/L.

This expression can be converted to a first-order rate expression if the concentration of hydroxide ion is known and is relatively constant. The hydroxide concentration is a function of pH, specifically $[OH^-] = K_w - 10^{-pH}$, where $K_w$ is the dissociation constant of water, which is a function of temperature (Fisher and Barnes, 1972). Available data suggest that the LDG reservoir pH measured at room temperature is between 7 and 8. Table 1 lists the values of $k$, $[OH^-]$, and the product $k[OH^-]$ as a function of temperature for the LDG reservoir, which were estimated by extrapolating the data of Robinson and Tester (1990) to obtain $k$ and calculating $[OH^-]$ assuming a reservoir pH of 8 measured at room temperature and using the temperature dependence of $K_w$ from Fisher and Barnes (1972). It was assumed that there was no significant buffering of pH, which can further complicate the calculations.

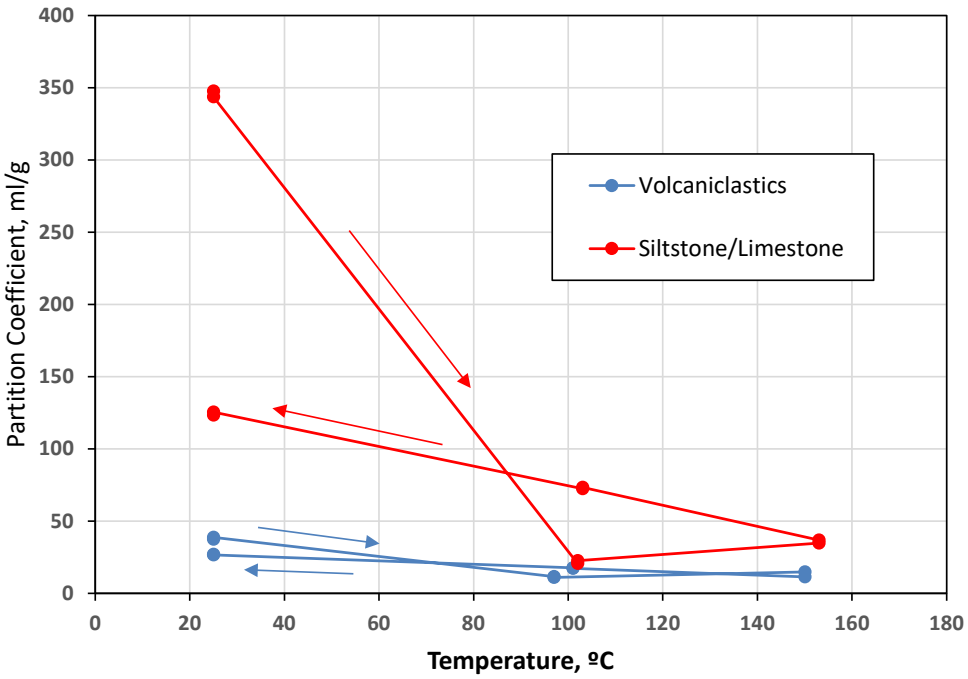


**Figure 3.** $Cs^+$ partition coefficients as a function of temperature and thermal hysteresis for the two different LDG lithologies tested. Arrows indicate direction of temperature cycling during experiments. There are two points at each temperature that correspond to replicate samples collected at a given time (most appear as a single point because of good agreement).

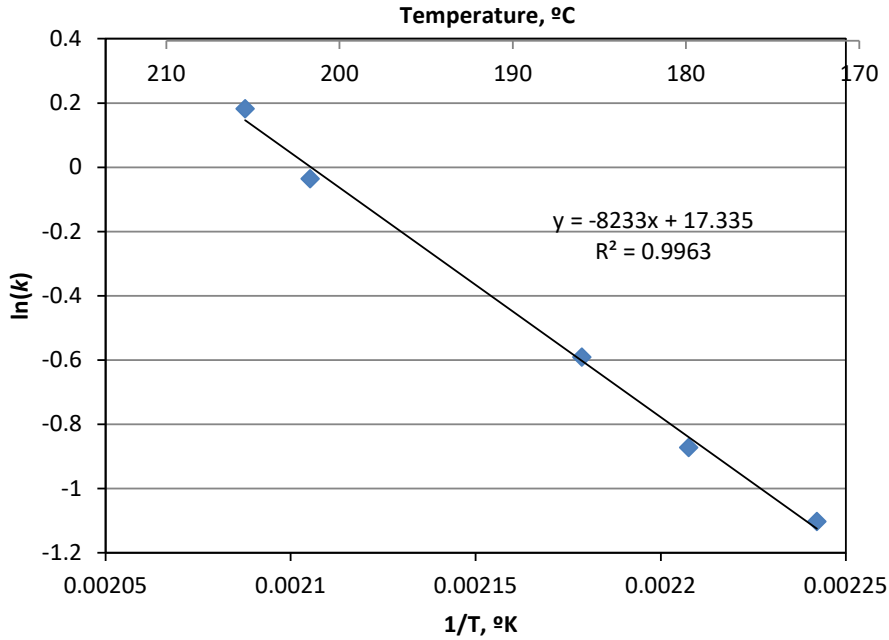


**Figure 4.** Arrhenius plot showing temperature dependence of second-order butyramide hydrolysis rate constant reported by Robinson and Tester (1990). Line is a linear regression fit to the data.

**Table 1.** Values of $k$ and $[OH^-]$ and the product $k[OH^-]$ as a function of temperature deduced from extrapolations of data of Robinson and Tester (1990).

| Temperature | $k$, L/mole-hr | $[OH^-]$, mole/L | $k[OH^-]$, $hr^{-1}$ |
|---|---|---|---|
| 100ºC | 31.5 | $7 \times 10^{-6}$ | $2.2 \times 10^{-4}$ |
| 125ºC | 126.2 | $1 \times 10^{-5}$ | $1.3 \times 10^{-3}$ |
| 150ºC | 428.5 | $1.4 \times 10^{-5}$ | $6.0 \times 10^{-3}$ |

Butyramide was selected from among the thermally-degrading tracers investigated by Robinson and Tester (1990) because it exhibited some of the slowest hydrolysis kinetics of any of the tracers. Its kinetics were slow enough that if temperatures remained near the injection water temperature (~100ºC in the 2017 test) in the flow pathways between well I and well P, there was not expected to be much degradation of the butyramide. However, if the temperatures approached or exceeded that of well P (~120ºC), significant degradation would be observed.

There are clearly uncertainties associated with applying the experimentally-determined $Cs^+$ partition coefficients and the calculated butyramide decay rate constants to interpret the 2017 reactive tracer test data. In the former case, it is highly optimistic to think that a single small rock sample (13-14 grams in each reactor) will accurately represent the $Cs^+$ partitioning behavior of all the rock surfaces along the flow pathways between wells I and P. Furthermore, the cuttings samples likely contained some fresh surfaces exposed by the drilling process that would not otherwise be present in the reservoir. In the case of butyramide, the experiments of Robinson and Tester (1990) were carried out in simple buffer solutions that do not represent the water chemistry in the LDG reservoir, and the experiments also did not include any rock surfaces, which could potentially alter the hydrolysis reaction kinetics. Furthermore, the butyramide experiments were conducted at much higher temperatures than at LDG, so the data had to be extrapolated to well below the range of observations.

### *2.2 Tracer Test Conduct*

The tracer test was initiated on Oct. 12, 2017, with simultaneous injection of all the tracers into well I within about 8 hours. Sampling of well P started that same day and ended on November 30, 2017. The tracer injection masses were 25 kg of sodium 1,5-naphthalene disulfonate, 100 kg of CsCl, and 500 kg of butyramide. The injections were accomplished by dissolving appropriate quantities of each tracer (in rough proportion to their injection masses) in several 350-gallon batches, and injecting each batch at a slow rate into the main injection flow stream routed to the well I wellhead using a high pressure pump to overcome the injection line pressure. The dilution provided by the much larger flow rate in the main injection stream ensured that the tracer concentrations in the injectate were low enough that density-driven flow as a result of concentration effects was not a concern (density contrast between traced and untraced water was less than 0.05%). Non-geothermal water was used to dissolve the tracers in 350-gallon plastic totes for each batch. The relatively low solubility and large quantity of butyramide was the rate-limiting factor for the injection process.

Because of concerns about cooling of well P, injection of spent geothermal water into well I began only a couple of hours before tracer injection commenced, and injection into well I was

conducted for only 7 days. The injection rate into well I was approximately 500 gallons per minute (gpm) at an average temperature of about 102ºC throughout all 7 days of the injection (ranging from 90 to 108ºC, with the temperature being around 107ºC during the tracer injection). The production rate from well P averaged 550 to 600 gpm over the first 14 days of the test, then decreased to about 500 gpm for ~3 days, and then increased to ~1000 gpm for the remainder of the test. The temperature in well P remained steady at 121-122ºC throughout the test.

After the tracers were injected, well P was sampled twice per day. The twice-per-day sampling of well P continued for approximately 2 weeks, after which it was reduced to once per day. Sampling was accomplished by opening a sampling port at the wellhead and routing the sample stream through a ¼" coiled stainless steel tube that was submerged in an ice bath to ensure that the sample remained condensed. Samples were collected in 4-oz plastic (LDPE) bottles and in 2-oz (60-ml) amber glass bottles fitted with Teflon-lined screw caps.

### *2.3 Tracer Analyses*

The samples were refrigerated at LDG and eventually shipped in coolers on ice to LANL for analysis. High-performance liquid chromatography (HPLC) with fluorescence detection was used to quantify the sample concentrations of 1,5-NDS. Quantification by emitted fluorescent light allows the tracer to be detected at concentrations less than 1 part per billion (ppb) or 1 μg/L. The HPLC separates the naphthalene sulfonates (NSs) chromatographically so that they can be analyzed by fluorescence without interfering with each other (the samples contained lingering concentrations of 2-NS, 2,6-NDS, 2,7-NDS, and 1,3,6-NTS from the 2016 tracer test and from another tracer test conducted earlier in 2017). The chromatographic separation is accomplished by eluting a sample containing multiple NSs through a C18 reverse phase Waters XBridge C18 3.5mm 4.6X50 column. The eluent is 70% 5 mM tetrabutyl ammonium phosphate (TBAP) in deionized water with a small amount of $K_2HPO_4$ added to buffer to a near-neutral pH and 30% 5 mM TBAP in HPLC-grade methanol. The TBAP serves as an ion-pairing agent that renders the negatively-charged NSs neutral so that they are retained in the reverse phase column. The method was adapted from a method provided by colleagues at the Energy and Geoscience Institute at the University of Utah. The NSs were detected using a Dionex FLD-3100 fluorescence detector set to excite at 222 nm and to measure fluorescence emission at 338 nm. The detector adjusted the gain and sensitivity automatically to optimize the signal-to-noise ratio for each sample. For each analytical run, a series of standards, typically spanning a range from 10 to 100 μg/L, was prepared from the original tracer stock powder. The results for these standards were used to translate peak area counts to concentrations for all the unknown samples.

Butyramide was analyzed using an HPLC method adapted from Elias et al. (2012) with UV absorbance detection at 200 nm. However, unlike Elias et al. (2012), we found that we did not have to pre-concentrate the samples by evaporation to quantify the butyramide. We suspect that this may be because our UV lamp/detector system was more efficient at 200 nm, which is at the low end of the wavelength range of most UV detectors (butyramide absorbance basically vanished above about 220 nm). Our quantification limit without pre-concentration was approximately 0.1 mg/L, although butyramide could be positively identified and concentrations qualitatively estimated in samples with concentrations less than 0.05 mg/L. The same HPLC hardware was used for both the naphthalene sulfonate and butyramide analyses, although different columns and eluents were employed for the two methods. Like the 1,5-NDS, a series of standards were prepared from the original tracer stock and analyzed for each analytical run to provide translation from peak area counts to concentrations.

$Cs^+$ was analyzed by Inductively Coupled Plasma-Mass Spectrometry using a Perkin-Elmer NexION 300S, following EPA method 200.8. The $Cs^+$ quantification limit was well below the background concentrations in the LDG samples, so unlike the other tracers, the challenge was to measure small elevations above background concentrations.

# 3. Tracer Test Results and Interpretations

## *3.1 Results*

Figures 5 and 6 show the tracer breakthrough curves as a function of time and as a function of volume produced in well P, respectively. Note that the tracer concentrations are normalized by dividing by their injection masses. Both figures show the times/volumes corresponding to the end of water injection into well I and the flow rate changes in well P. The tail of the breakthrough curves look longer in Figure 6 because the production rate from well P increased later in the test, so there was more volume produced per day later in the test. Note that the $Cs^+$ concentrations in Figure 5 are not background subtracted, but they are background subtracted in Figure 6. Figure 7 shows the actual $Cs^+$ concentrations in well P throughout the test, and it is apparent that the concentrations were decreasing slightly, although the variation is extremely small; i.e., a range of about 8 μg/L for all measurements. The high level of precision with very little random scatter should have made it possible to distinguish even a very minor breakthrough of injected $Cs^+$ from the background trend. It is apparent that a $Cs^+$ breakthrough did not occur.

The normalized breakthrough curves of the 1,5-NDS in Figures 5 and 6 were adjusted upward slightly so that they had approximately the same normalized peak concentration as the butyramide. Without this adjustment, the normalized concentration of butyramide was about 12% higher than that of the 1,5-NDS. This is technically not possible because the 1,5-NDS is known to be nonreactive (Rose et. al., 2001), and butyramide is a smaller molecule than NDS, so it should have a larger diffusion coefficient that would result in more of it diffusing out of flowing fractures and into the rock matrix than the NDS if such diffusion were significant. The discrepancy is likely due to some difference in the purity of the two tracers or more likely systematic errors in the preparation of standards for the analytical measurements of the tracers. The purity of the butyramide was stated to be 99.6% on its certificate of analysis. The naphthalene sulfonates are typically much less pure, often 95% or less. Lower purity of the 1,5-NDS would cause its normalized breakthrough curve to be artificially low. Standards do not exist for either the 1,5-NDS or butyramide, so as discussed in the preceding section, they had to be prepared from the bulk starting materials. Normally, this should negate some of the errors caused by impurities because the impurities should effectively be incorporated into the standards. However, only very small amounts of tracer material are needed for standards, and such small amounts can result in nonrepresentative sampling of the bulk material, which could result in a greater or lesser fraction of impurities in the standards than in the bulk material. In effect, we considered the 1,5-NDS injection mass to be 22 kg instead of 25 kg so that the peak of its normalized breakthrough curve approximately coincided with the peak of the butyramide breakthrough curve.

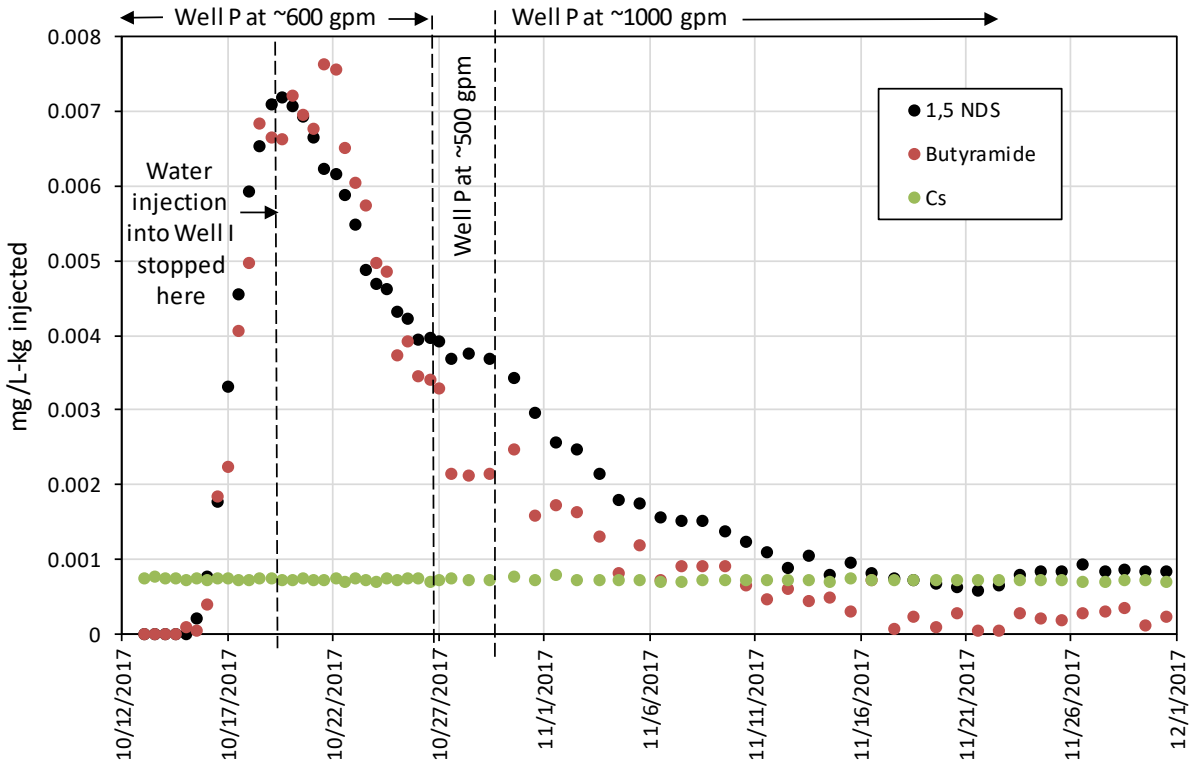


**Figure 5.** Normalized tracer breakthrough curves as a function of time with 1,5-NDS corrected.

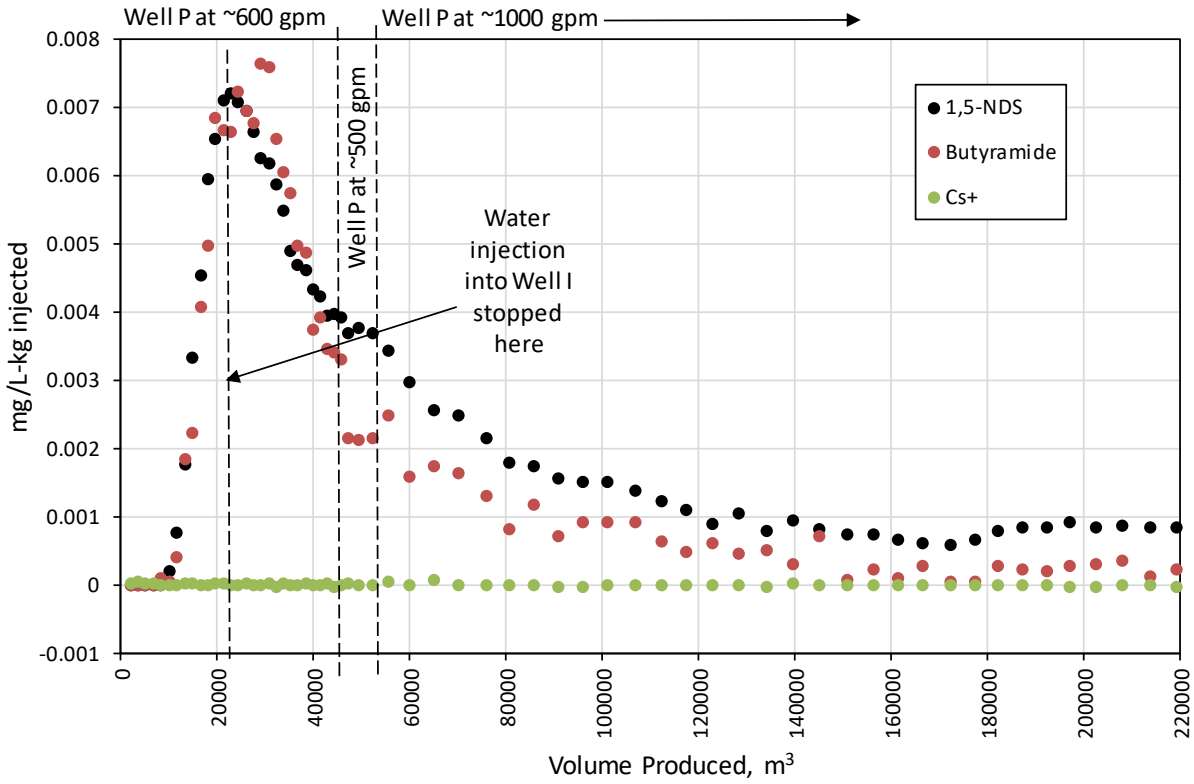


**Figure 6.** Normalized tracer breakthrough curves as a function of volume produced from well P with 1,5-NDS corrected. $Cs^+$ concentrations are background-subtracted.

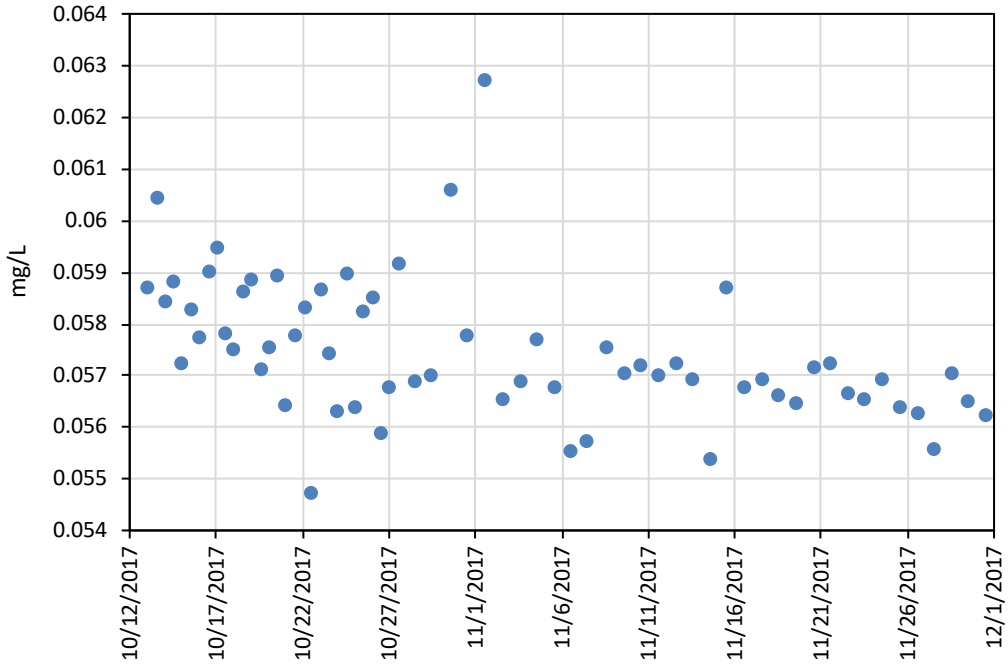


**Figure 7.** $Cs^+$ concentrations in well P throughout the tracer test.

### *3.2 Interpretations*

The RELAP model described in Reimus et al. (2003, Appendix A) was used to interpret the tracer test results. The interpretive procedure involved first matching the 1,5-NDS breakthrough curve, assuming the 1,5-NDS was nonreactive. The model was matched separately to the breakthrough curves as a function of volume produced and as a function of time (i.e., to the curves of Figures 5 and 6, respectively). Matching the curve as a function of volume produced is normally the preferred approach to obtain flow pathway volumes when the production flow rate varies, as it did in the tracer test. However, because the thermal degradation rate of the butyramide and the diffusion rates of the tracers are time-dependent processes, it was also necessary to obtain a match to the time-dependent curves so that the butyramide and $Cs^+$ responses (or lack thereof in the case of the $Cs^+$) could be properly interpreted.

RELAP uses the 1-D advection-dispersion equation to match tracer breakthrough curves, and it has the capability to account for diffusive mass transfer of tracers between flowing water in fractures and stagnant water in the rock matrix that is in communication with the fractures. Frequently, the shapes of breakthrough curves are such that a single flow pathway (having a single mean residence time and a single dispersion coefficient) does a poor job of fitting an entire breakthrough curve. When this occurs, it is reasonable to assume that the breakthrough curve is the result of multiple flow pathways, or sets of flow pathways, each of which have a contribution to the overall breakthrough curve. In matching the 1,5-NDS breakthrough curve, it was found that three pathways, or sets of pathways, were needed to obtain a good match to the observations. The resulting matches to the volume- and time-dependent curves are shown in Figures 8 and 9, respectively. The model parameters used to obtain these matches are listed in Table 2. The parameters for the volume-dependent curve match should be used for the best estimates of the

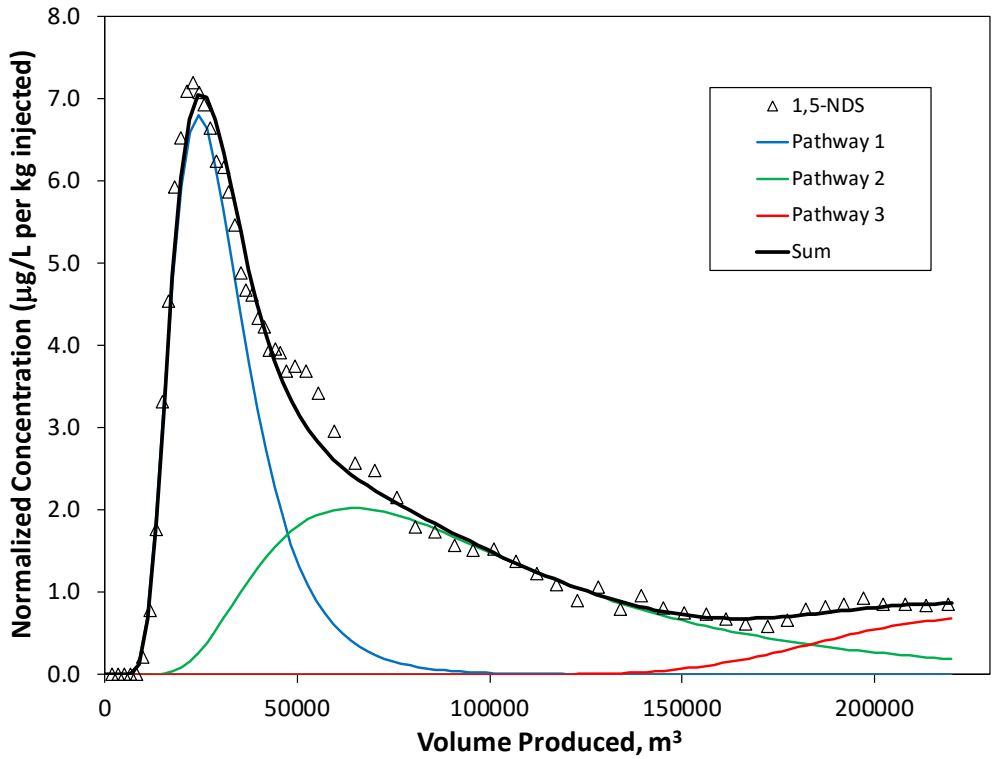


**Figure 8.** Multiple-pathway RELAP model fit to 1,5-NDS concentration vs. volume produced.

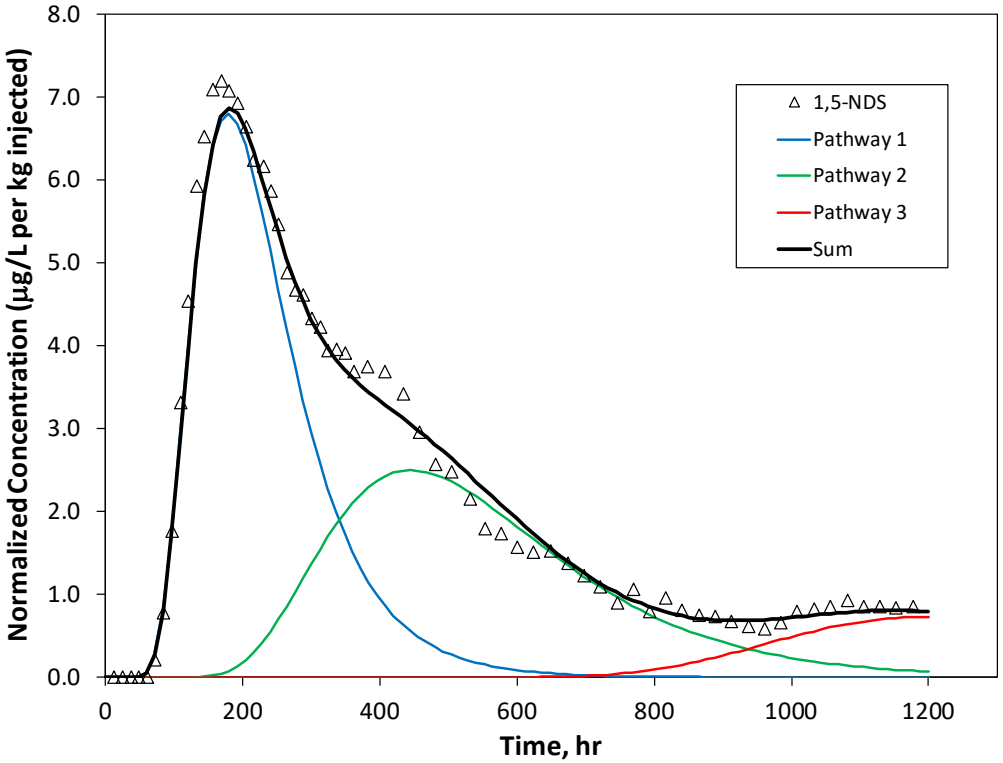


**Figure 9.** Multiple-pathway RELAP model fit to 1,5-NDS concentration vs. time.

**Table 2.** Model parameters yielding the RELAP model curves of Figures 8 and 9.

**Concentrations vs. Volume Produced**

| Parameter | Pathway 1 | Pathway 2 | Pathway 3 |
|---|---|---|---|
| Tracer Mass Fraction | 0.175 | 0.21 | 0.08 |
| Mean Volume, $m^3$ | 30,000 | 102,500 | 240,000 |
| Peclet Number* | 12 | 6 | 50 |

**Concentrations vs. Time**

| Parameter | Pathway 1 | Pathway 2 | Pathway 3 |
|---|---|---|---|
| Tracer Mass Fraction | 0.175 | 0.15 | 0.06 |
| Mean Residence Time, hr | 220 | 540 | 1250 |
| Peclet Number* | 12 | 14 | 50 |

*Peclet number = transport distance divided by longitudinal dispersivity.

Note: Matrix porosities, fracture half apertures, diffusion distances into the matrix, and matrix diffusion coefficients were 0.05, 0.1 cm, 0.02 cm, and $1x10^{-6}$ cm2/s, respectively in all simulations. These parameters are not unique to the model curves; they served to suppress matrix diffusion.

fraction of tracer mass traveling in each flow pathway. These estimates are lower for the two longer flow pathways in the case of the time-dependent breakthrough curves because the times are compressed relative to the volumes produced later in the test. Note that the parameters affecting diffusion of the tracer out of fractures and into the matrix (i.e., matrix porosity, fracture half aperture, and matrix diffusion coefficient) are not uniquely determined by the model. These parameters were set to values that limit the diffusive mass transfer between fractures and matrix so that it has a relatively small effect on the 1,5-NDS breakthrough curve. The rationale was that any significant diffusive mass transfer would have resulted in a noticeable lowering of the normalized butyramide peak concentration as well as a difference in the shape of the butyramide breakthrough curve relative to the normalized 1,5-NDS curve, and neither feature was observed.

The model parameters obtained for the time-dependent breakthrough curve matches (listed in Table 2) were assumed to apply to both the butyramide and $Cs^+$ because these tracers were injected simultaneously with the 1,5-NDS, and therefore they should have followed the same flow pathways in the same proportions as the 1,5-NDS. The only parameter that was adjusted to match the butyramide breakthrough curve was the first-order thermal decay rate constant; i.e., $k[OH^-]$ in Table 1. Figure 10 shows the match of the model to the time-dependent butyramide data, and Table 3 lists the rate constants and associated inferred temperatures in each of the flow pathways deduced for the 1,5-NDS tracer (obtained from extrapolation of the data of Robinson and Tester, 1990). The temperatures must be low (100ºC or less) in the fastest flow pathway because there is very little or no observed decay of the butyramide relative to the 1,5-NDS, and even an assumed temperature of 100ºC results in a very slight lowering of the predicted normalized butyramide breakthrough curve. The second and third flow pathways clearly exhibit lower normalized concentrations of butyramide relative to the 1,5-NDS, and the temperature in both pathways is deduced to be approximately 120ºC. However, the contribution of the third pathway is relatively minor, and consequently the uncertainty in the deduced temperature in this pathway is larger than in the case of the second pathway.

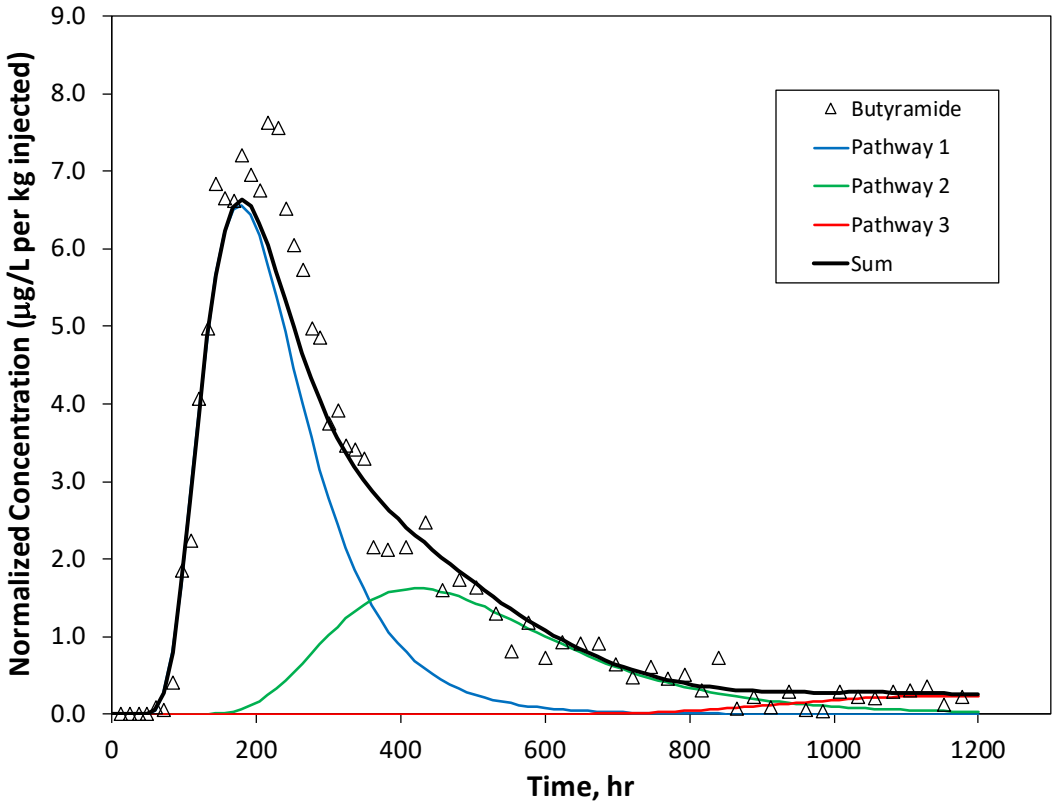


**Figure 15.** Multiple-pathway RELAP model fit to butyramide breakthrough curve.

**Table 3.** Values of $k[OH^-]$ and pathway temperatures inferred from RELAP model matches to the butyramide breakthrough curve shown in Figure 15.

| Parameter | Pathway 1 | Pathway 2 | Pathway 3 |
|---|---|---|---|
| $k[OH^-]$, $hr^{-1}$ | 0.0002 | 0.001 | 0.001 |
| Inferred Temperature, ºC | ≤100 | 120 | 120 |

Because the $Cs^+$ did not appear at all in production well P, the interpretation of its transport behavior is limited to estimating model parameters that would prevent it from reaching well P in measurable concentrations. For this exercise, we assumed that the transport of tracers occurred almost exclusively in fractures, and we used the adsorption partition coefficient measured for the volcaniclastic rocks at 100ºC (~15 ml/g) to describe $Cs^+$ interaction with the rocks. While it is possible that the tracers could have also traveled through the underlying siltstone or even the deeper limestone, this seems rather unlikely given the configuration of the injection and production wells, shown in Figure 2, and furthermore, even if this were the case, a significant fraction of the transport distance would necessarily have to be in the volcaniclastics. Because there are no good estimates of fracture apertures, matrix porosities or maximum distances of diffusion into the matrix available for the LDG reservoir, we assumed combinations of these parameters that ensured that the breakthrough curves of 1,5-NDS and butyramide were not

significantly affected by matrix diffusion. These constraints either kept matrix porosities very low or matrix diffusion distances very short. Treating a cation-exchanging tracer as if it is adsorbing in the matrix after diffusing only a very short distance into the matrix is consistent with observations made in porous medium column experiments at elevated temperatures (Dean et al., 2015; Reimus et al., 2018), so these assumptions seem reasonable.

Table 4 lists some of the combinations of fracture half apertures, matrix porosities, and diffusion distances in each of the first two flow pathways that resulted in a predicted increase of approximately 5 μg/L of $Cs^+$ in well P by the end of the tracer test. We note that for parallel-plate fractures, the fracture half aperture is equivalent to the water volume to surface area ratio, so in the ensuing discussion, the fracture half aperture can be thought of as the inverse of the surface area to volume ratio in flowing fractures. For any given combination, a larger half aperture, a smaller matrix porosity, or a shorter diffusion distance will result in a greater increase in $Cs^+$ than 5 μg/L. Given that the full range of measured $Cs^+$ concentrations in well P was less than 8 μg/L (and the observed trend was slightly downward), an increase of 5 μg/L of $Cs^+$ by the end of the test should have been observable. To illustrate this, Figure 11 provides an example of one of the predicted $Cs^+$ breakthrough curves superimposed on the actual measured concentrations. In essence, Table 4 lists the *maximum* fracture half-aperture associated with each listed matrix porosity and range of diffusion distances that is compatible with the lack of a $Cs^+$ breakthrough. The third flow pathway was not considered because its contribution is so late in the test and so low in concentration, that almost any adsorption behavior of $Cs^+$ would have resulted in no predicted $Cs^+$ contribution from this pathway before the end of the test.

**Table 4.** Combinations of values of fracture half-aperture, matrix porosity, and diffusion distance into the matrix that yield predicted $Cs^+$ concentration increases of 5 μg/L by the end of the tracer test.

| First Flow Pathway | | |
|---|---|---|
| **Fracture half-aperture, cm** | **Matrix porosity** | **Diffusion distance, cm** |
| 0.06 | 0.01 | >0.05 |
| 0.13 | 0.05 | 0.11-0.37 |
| 0.18 | 0.1 | 0.16-0.27 |
| 0.23 | 0.2 | 0.2-0.22 |
| **Second Flow Pathway** | | |
| **Fracture half-aperture, cm** | **Matrix porosity** | **Diffusion distance, cm** |
| 0.17 | 0.01 | >0.05 |
| 0.37 | 0.05 | 0.14-0.45 |
| 0.51 | 0.1 | 0.16-0.49 |
| 0.68 | 0.2 | 0.25-0.42 |

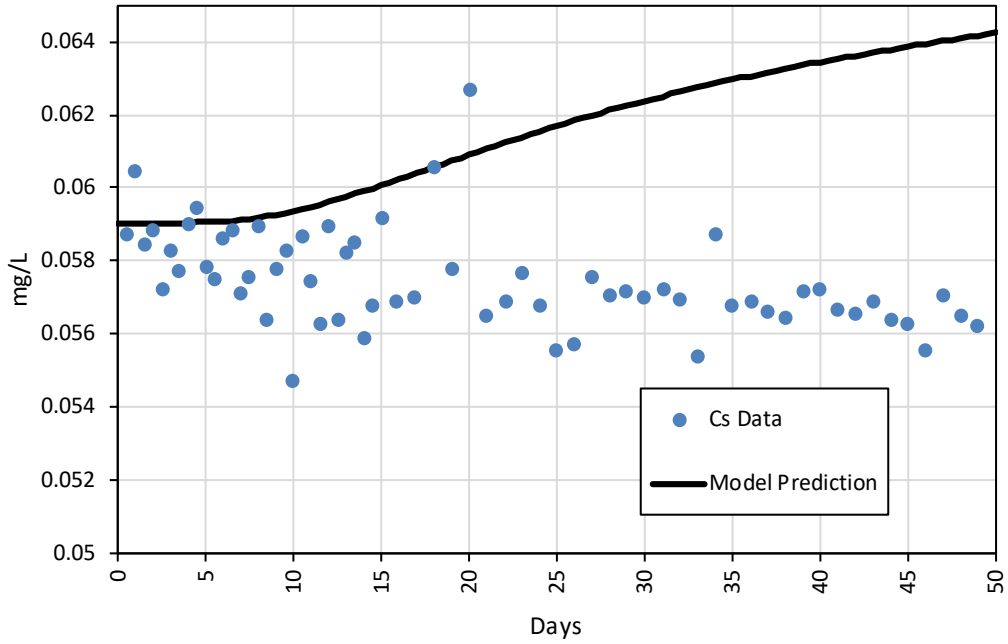


**Figure 11.** Predicted breakthrough curve of $Cs^+$ that was considered to correspond to a definitive elevation (0.005 mg/L) of $Cs^+$ concentrations above the baseline trend in well P (blue dots).

From Table 4 it is apparent that the fracture half apertures yielding increases in $Cs^+$ concentrations similar to that shown in Figure 11 are not extremely sensitive to assumed values of matrix porosity (they vary approximately in proportion to the square root of matrix porosity). This result can be attributed to a complex interplay of the parameters governing both matrix diffusion and $Cs^+$ adsorption. When the matrix porosity is increased, the maximum diffusion distance must decrease to maintain a 1,5-NDS breakthrough curve that does not have too much matrix diffusion. Also, a larger matrix porosity results in less rock mass per unit volume of water for $Cs^+$ adsorption in the matrix, and consequently the effective $Cs^+$ retardation factor in the matrix decreases. The net results of the combination of a larger matrix porosity, shorter diffusion distance, and a decreased $Cs^+$ retardation factor in the matrix is that the increases in fracture half aperture necessary to meet the constraints provided by the 1,5-NDS and $Cs^+$ observations are given by the square root dependence on matrix porosity mentioned above. The half-apertures estimated for the second flow pathway are about 3 times larger than those for the first pathway for the same assumed matrix porosity. This is primarily a consequence of the longer travel time in the second pathway, which forces this pathway to have less diffusive mass transfer (i.e., a larger half aperture for the same matrix porosity) to achieve a similar increase in $Cs^+$ concentrations by the end of the test as for the first pathway.

## 4. Predictions of Thermal Drawdown

It can be shown that heat transfer rates between hot rock and water in geothermal reservoirs are inversely proportional to water volume to surface area ratios or fracture half apertures (Section 4.2 of Williams et al., 2013). The fracture half apertures of Table 4 represent

reasonable estimates of *upper bounds* that are compatible with the lack of a $Cs^+$ breakthrough in the 2017 tracer test. However, timing of thermal drawdown also depends on the volume of rock from which heat is being extracted per unit volume of heat extracting water. For the same surface area to water volume ratio in a fracture system, thermal drawdown will occur faster if fractures are spaced more closely together. Reactive tracers do not provide an estimate of fracture spacing. However, if the total volume of reservoir (including both rock and water) through which water is flowing between an injection and production well is known (or estimated), then an average fracture spacing can be estimated from the average fracture aperture determined from an adsorbing tracer and the flowing pathway volume estimated from a nonreactive tracer. Specifically, the average fracture spacing is estimated as the average fracture aperture divided by the ratio of flowing pathway volume to total volume (i.e., the flowing porosity). The flowing pathway volume is estimated as $fV(Q_{inj}/Q_{prod})$, where $f$ and $V$ are the nonreactive tracer mass fraction and mean production volume associated with the pathway, respectively (taken from Table 2 for pathways 1 and 2 between wells I and P), and $Q_{inj}$ and $Q_{prod}$ are the injection and production flow rates, respectively. For flow pathways 1 and 2, the pathway volumes are calculated as approximately 4400 $m^3$ and 17,900 $m^3$, respectively. If the volume of reservoir through which water is flowing between wells I and P is taken to be a block that is 1000 ft long (20% more than the horizontal distance between the wells to allow for some "flare" around the injection well) by 600 ft thick (the approximate vertical distance from the bottom of well I to the top of the open interval in well P) by 100 ft wide, then the total volume is ~1,700,000 $m^3$. The flowing porosities associated with flow pathways 1 and 2 are then estimated to be about 0.0025 and 0.01, respectively. The 100 ft width of the reservoir block may seem rather narrow, but it allows for the likelihood that the fractures are clustered in narrow zones rather than being evenly spaced throughout the entire block. Clustering will result in smaller average fracture spacings and thus more rapid thermal drawdown, so assuming a narrow block width is conservative. By using this approach to estimate fracture spacings, the average fracture spacing will always be directly proportional to the average fracture aperture (i.e., the ratio of the two will be the same). For flow pathway 1, the fracture spacing will be 400 times the fracture aperture, and for pathway 2, the spacing will be 100 times the aperture.

Section 4.1 of Williams et al. (2013) describes a semi-analytical model based on the RELAP model (Reimus et al., 2003) that can predict thermal drawdown in geothermal reservoirs assumed to consist of parallel, constant-aperture fractures that are evenly spaced. The model is used here to predict thermal drawdown between wells I and P at the LDG site using the information obtained from the tracer test. Besides the tracer-derived data, the model also requires the thermal conductivity, heat capacity (or specific heat), and density of the rock, as well as the heat capacity and density of water, as inputs. For this exercise, a thermal conductivity of 0.01 W/cm-K, a heat capacity of 0.9 J/g-K, and a density of 2.65 $g/cm^3$ were assumed for the rock. These values are reasonable for a volcaniclastic rock, although the thermal conductivity can vary from less than 0.004 W/cm-K to as much as 0.02 W/cm-K, depending on a variety of factors (Lenhardt and Gotz, 2015). The heat capacity and density of water were taken to be 1 $g/cm^3$ and 4.19 J/g-K, respectively.

Figures 12 and 13 show thermal drawdown curves predicted for flow pathways 1 and 2, respectively, between wells I and P. The temperatures on the y-axes are normalized to show a decreasing trend at well P from the initial flow pathway temperature to the injection water temperature. In each figure, curves are shown for the largest and smallest of the fracture half apertures listed in Table 4, and also for two much larger fracture apertures for which thermal

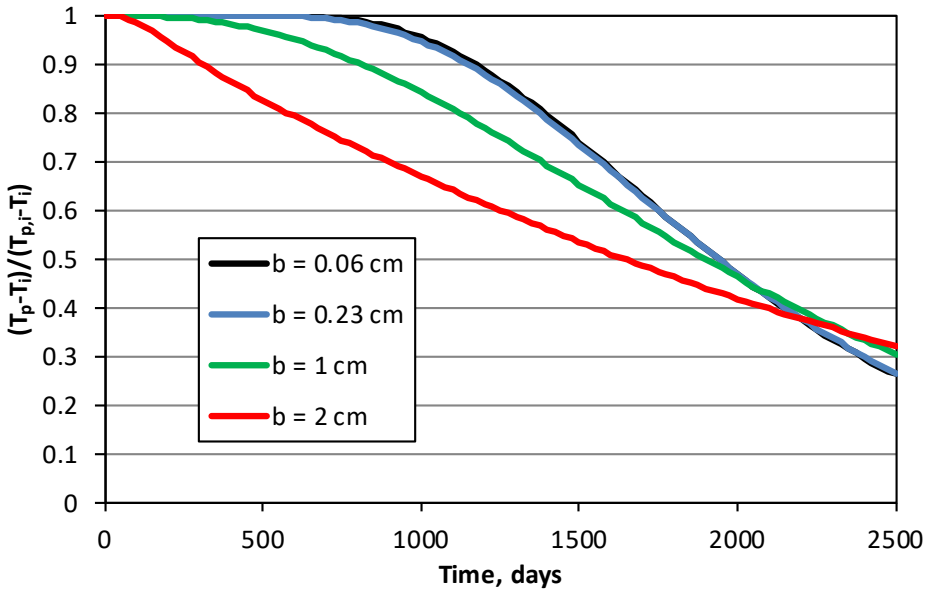


**Figure 12.** Predicted normalized temperature at exit of pathway 1 (exiting into well P) as a function of time (assuming 500 gpm injection and production rates). $T_p$ = temperature at exit of pathway, $T_i$ = injection water temperature, $T_{p,i}$ = initial average temperature in pathway.

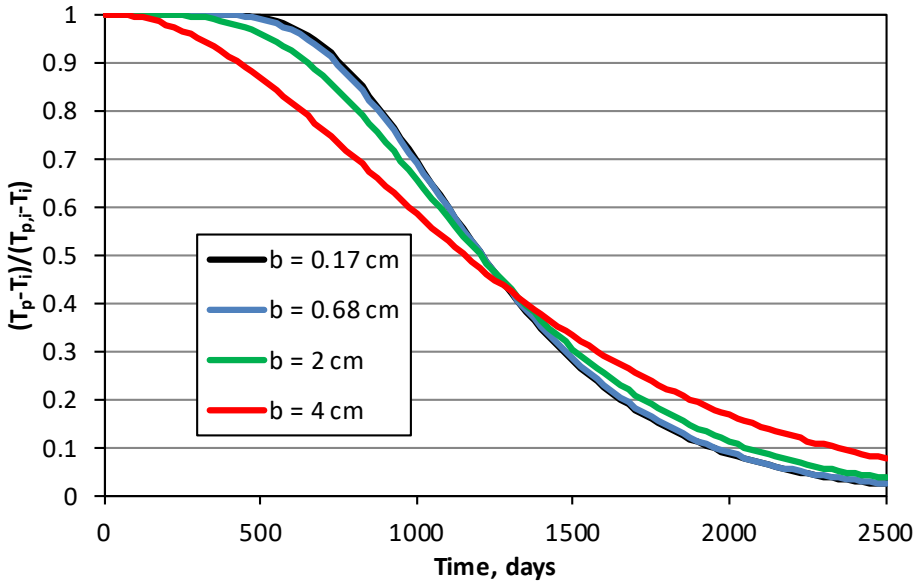


**Figure 13.** Predicted normalized temperature at exit of pathway 2 (exiting into well P) as a function of time (assuming 500 gpm injection and production rates). $T_p$ = temperature at exit of pathway, $T_i$ = injection water temperature, $T_{p,i}$ = initial average temperature in pathway.

drawdown is predicted to occur notably sooner. It is apparent that there is little sensitivity of the predicted thermal drawdown time to fracture half aperture over the range of fracture half apertures in Table 4 (which are *maximum* apertures listed as a function of matrix porosity). This result is obtained because the thermal drawdown time is primarily dependent on the ratio of

water volume to rock volume within the block of rock being cooled (i.e., the flowing porosity) *until* the fracture aperture exceeds some critical value. The critical value is a function of the water residence time in the pathway, with the value decreasing as residence time decreases. It is apparent from Figures 12 and 13 that the critical half-aperture values for flow pathways 1 and 2 are approximately 1 cm and 2 cm, respectively. Thus, the establishment of upper bounds for the fracture half-apertures in flow pathways 1 and 2 that are less than the critical values (because of the lack of a $Cs^+$ breakthrough) effectively indicates that the flow pathways are in a regime where the thermal drawdown time is sensitive mainly to the flowing porosity, not the apertures. Of course, the thermal drawdown time will also be sensitive to the thermal properties of the rock, but the flowing porosity is far more uncertain than the rock thermal properties.

The preceding paragraph addresses the timing of thermal drawdown at well P, but it does not address the magnitude of the drawdown. To estimate the magnitude of thermal drawdown at well P, we can use the pathway temperatures estimated from the thermally-decaying tracer breakthrough curve in conjunction with the mass fractions of nonreactive tracer associated with each flow pathway. Although the final temperature within a given flow pathway will always approach the injection water temperature (if water is injected long enough), the effect on the production well temperature will also depend on the fraction of flow into the production well that is being contributed by the flow pathway. The following equation describes this dependence for a given pathway:

$$\Delta T = T_{Prod,f} - T_{Prod,i} = -f \frac{Q_{inj}}{Q_{prod}} \left(T_{path,i} - T_{inj}\right) \qquad (2)$$

where, $T_{Prod,f}$ = final temperature in production well after complete thermal drawdown in flow pathway, ºC

$T_{Prod,i}$ = initial temperature in production well, ºC

$f$ = fraction of tracer mass following flow pathway

$T_{path,i}$ = initial average temperature in flow pathway, ºC

$T_{inj}$ = injection water temperature, ºC

$Q_{inj}$, $Q_{prod}$ = injection and production flow rates, respectively

The analysis of the butyramide breakthrough curve provided an estimated average temperature in flow pathway 1 that was no greater than 100ºC, and estimated average temperatures in flow pathways 2 and 3 that were both about 120ºC. These can be taken to be initial flow pathway temperatures because well I had not been used as an injection well for nearly a year when the tracer test started, and furthermore it was used as an injection well for only a few months in 2016 after bringing well P online as a production well. Interestingly, if the average temperature in flow pathway 1 is 100ºC and the injection water temperature into well I is 100ºC (as it was during the tracer test), then equation (2) predicts that the impact of flow pathway 1 on the temperature in well P will be negligible because there will be no net heat transfer. Of course, the butyramide cannot distinguish between a temperature of 100ºC and a lower temperature because it would take temperatures greater than 100ºC to result in any appreciable decay in pathway 1. If we assume an initial temperature of 80ºC in pathway 1, an injection water temperature of 100ºC, an initial production well temperature of 120ºC, and a total injection flow rate equal to the production flow rate (approximately the case in the tracer test), then $\Delta T$ in equation (2) will be -3.5ºC. If we take 120ºC to be the initial temperature in pathway 2, then $\Delta T$ for pathway 2 is calculated to be -4.2ºC, and if pathway 3 is lumped with pathway 2

(because they both have the same temperature) then the combined $\Delta T$ for these pathways is estimated to be -5.8ºC. For the case of thermal drawdown in well P caused by injection of 100ºC water into well I, the maximum temperatures in Figures 12 and 13 would both be 120ºC (the initial production well temperature), and the minimums would be 116.5ºC in Figure 12 and 115.8ºC in Figure 13 (for pathway 2 alone).

Given the information on timing of thermal drawdown provided (in a bounding way) by the $Cs^+$ breakthrough curve, as reflected in Figures 12 and 13, and the information on magnitude provided by the butyramide and nonreactive tracer responses, as reflected using equation (2), we can readily provide a prediction of the composite thermal drawdown at well P. This prediction is simply the sum of the two thermal drawdowns as a function of time and is shown in Figure 14 (with specific temperatures provided, and assuming that pathway 1 has an initial temperature of 80ºC). In Figure 14 we have conservatively included a magnitude contribution from the combination of pathways 2 and 3, with a timing that is associated with pathway 2. In reality, the timing for the pathway 3 contribution is likely to be later than for pathway 2 because of its greater water residence time. However, pathway 3 makes a relatively minor contribution because it only accounts for 8% of the nonreactive tracer mass fraction (vs. 21% for pathway 2).

It should now be clear that a reactive tracer that interrogates surface area to volume ratios can help constrain the timing of thermal drawdown, but not the magnitude of the drawdown (although the maximum possible magnitude is the difference between the production well temperature and the injection water temperature multiplied by the ratio of injection to production flow rates). Similarly, a thermally-decaying tracer can constrain the magnitude of thermal drawdown, but not the timing. Using both together is thus complementary in that it can provide estimates of both timing and magnitude of thermal drawdown. Both tracers must be used in conjunction with a nonreactive tracer to be properly interpreted, and the nonreactive tracer also

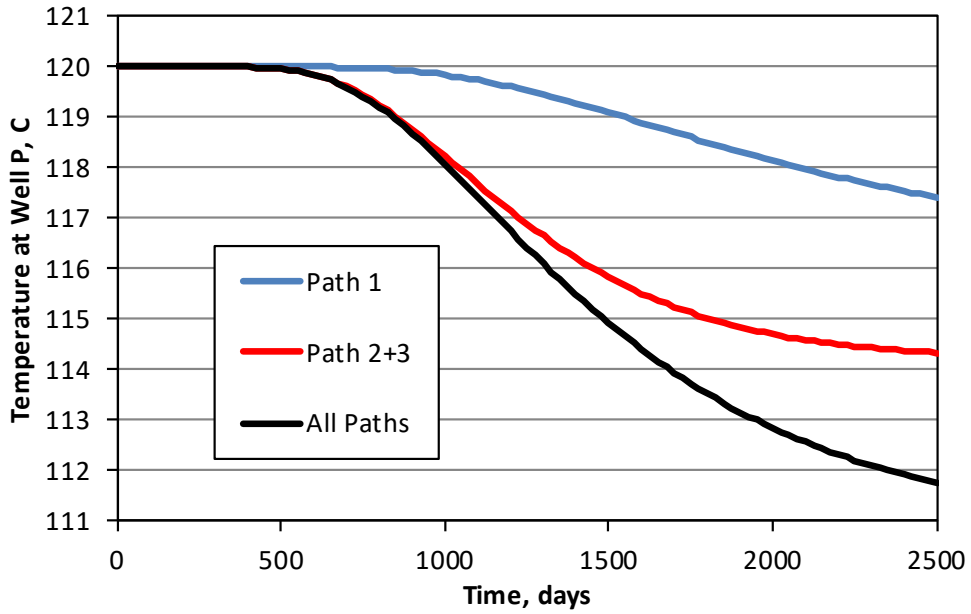


**Figure 14.** Predicted temperatures in well P as a function of time, showing contributions of thermal drawdown from flow pathway 1 and from flow pathways 2 + 3 (assuming 500 gpm injection and production rates).

provides information on mass fractions of water following different flow pathways, which factors into the magnitude estimates.

## 5. Discussion

The predictions of timing and magnitude of thermal drawdown between an injection well and a production well have many uncertainties and limitations. The main uncertainties and how they might be addressed are discussed in this section.

Regarding the interpretations of the reactive tracer breakthrough curves, there are inherent uncertainties that factor indirectly into the predictions of thermal drawdown. The interpretations of thermally-decaying tracer breakthrough curves rely on having good thermal degradation rates as a function of temperature. In using butyramide at LDG, we relied on the data of Robinson and Tester (1990), which involved an extrapolation of their thermal decay constants to lower temperatures and an assumption that the extrapolated decay rates in their experimental buffer solution and in the absence of rock surfaces would be the same as in the LDG reservoir. It was also assumed that the pH of the reservoir was 8 (at room temperature), but in reality pH measurements have varied from slightly less than 7 to somewhat greater than 8, and every change of one unit in pH translates to approximately an order of magnitude difference in the degradation rate constant at a given temperature. Obviously, these uncertainties could be greatly reduced by conducting thermal degradation experiments using geothermal water from LDG in contact with representative rocks from the reservoir. Such experiments could be conducted in the same apparatus that was used for the $Cs^+$ adsorption experiments described in Section 2.1. In the case of using $Cs^+$ as an adsorbing tracer, there is considerable uncertainty associated with using the measured sorption partition coefficients because of the potential non-representativeness of the small amounts of rock used in the experiments relative to the large amounts of rock encountered along the reservoir flow pathways. This uncertainty would probably best be reduced by conducting a set of column experiments at temperatures very close to those deduced in the flow pathways. Examples of such experiments are reported by Dean et al. (2015) and Reimus et al. (2018). These experiments have a significant advantage over the batch experiments described in Section 2.1 in that they have rock surface area to volume ratios that are much larger and therefore closer to what is expected in the reservoir. They also require much larger quantities of rock material, which should provide better representation of mineralogical variability in the rocks. Of course, one can never be entirely sure that any rock sample, no matter how large, is truly representative of the mineralogy and mineral alteration that exist along flow pathways that are over 1000 feet long and potentially span multiple lithologies.

We note that while the butyramide was effective in providing estimates of the temperatures in the second and third flow pathways, it was not optimal for estimating temperatures in the first pathway because it did not exhibit any apparent thermal decay in this pathway. That is, the temperatures in the first pathway could be cooler than 100ºC and still be consistent with the observed butyramide breakthrough curve. A different tracer that decays at lower temperatures would be more useful for interrogating the temperatures in the first flow pathway. Such a tracer could be selected from the suite of compounds that were evaluated by Robinson and Tester (1990).

In addition to uncertainties associated with tracer properties, there are additional uncertainties associated with a lack of information about the reservoir, and specifically about the geometry of

flow pathways in the reservoir. For the most part, these uncertainties cannot be addressed by tracers; they can only be addressed by careful consideration of well logs, core and cuttings, geophysical surveys, and general knowledge of site geology. Perhaps the greatest of these uncertainties is the uncertainty in knowing the average fracture spacing, which has a big impact on predicting the timing of thermal drawdown. In the predictions of the preceding section, a reservoir block volume was assumed, and the estimated volumes of flowing pathways were divided by this block volume to obtain flowing porosity estimates associated with the pathways. The average fracture spacings within the pathways were then estimated by dividing fracture aperture estimates by the flowing porosity estimates. Also, the fracture spacings were assumed to be constant within a given pathway. In reality, fractures are likely to be clustered into fracture sets, and both spacings and matrix block sizes are likely to be highly variable within a flow pathway, which imparts a great deal of uncertainty to predictions of the timing of thermal drawdown. The analysis above is considered somewhat conservative from the standpoint of yielding flowing porosity estimates of 0.25% and 1% in flow pathways 1 and 2, respectively, which are considered quite large for fractured systems, thus resulting in conservatively small estimates of average fracture spacings. However, if there are relatively narrow bands of highly fractured rock that transport much of the water between the injection and production wells, then the times to thermal drawdown might still be overestimated.

The possibility also exists that a portion of the flow pathways could have consisted of porous media rather than fractures. The heat in small grains or blocks of rock in porous media will be rapidly transferred to water flowing past it, so thermal drawdown can potentially occur very rapidly in porous media. For typical rock and water heat capacities, the thermal drawdown pulse in a section of porous media having 20% porosity would travel only about 3.5 times slower than the water itself (about 7 times slower if the porosity were 10%). Such rapid propagation of lower temperatures would result in rapid thermal drawdown in a production well. This possibility cannot be ruled out at LDG, and thus the rapid nonreactive tracer response in the 2016 tracer test was enough to prompt a decision to not use well I for injection as long as well P is in use as a production well.

Porous media within flow pathways could also cause errors in the upper bound estimates of average fracture apertures deduced from the lack of a $Cs^+$ breakthrough. Even a small amount of transport through porous media could have significantly retarded the $Cs^+$ such that it would not have arrived at well P even if fracture apertures in the majority of the flow pathways were quite large. Using the partition coefficient of the $Cs^+$ to the volcaniclastics (15 ml/g), $Cs^+$ would be predicted to travel through a section of porous media having 20% porosity at a rate that is approximately 150 times slower than the rate of water movement (and about 350 times slower if the porosity were 10%). Thus, any amount of porous media flow could cause the fracture aperture estimates of Table 4 to be low.

One possibility for estimating the timing of thermal drawdown that does not rely explicitly on reservoir geometry assumptions is the use of a thermally-decaying tracer at *two different times* during the operation of an injection-production well pair, ideally first when the well pair goes into operation (to estimate initial temperatures), and then again before thermal drawdown occurs. This possibility was explored in detail in Section 4.2.2 of Williams et al. (2013). If an average flow pathway temperature is estimated when a well pair is first brought on line, and then again at some later time, a geometry-independent estimate of the thermal drawdown time can, in principle, be obtained from:

$$t_{thermal} = \left(\frac{T_1 - T_{inj}}{T_1 - T_2}\right)(t_1 - t_2) \quad (3)$$

where, $t_{thermal}$ = time to thermal drawdown, days

$T_1$ = average temperature deduced from first test (close to initial pathway temperature), ºC

$T_2$ = average temperature deduced from second test, ºC

$T_{inj}$ = injection water temperature, ºC

$t_1$ and $t_2$ = times of tests 1 and 2, respectively, in total days since start of first test.

Equation (3) assumes that the injection and production flow rates and the injection water temperature remain reasonably constant over time (note that injection or production volume could be substituted for time if the flow rates vary but otherwise have a similar ratio over time). Also, equation (3) technically gives the time at which the average flow pathway temperature is predicted to be equal to the injection water temperature. In reality, temperatures will begin dropping at the production well before this occurs. The timing and magnitude of early temperature drop at the production well will depend on many factors, including dispersion in the flow pathways and the details of the geometry of the flow pathways, but all things considered, equation (3) should yield a reasonably good estimate of time to thermal drawdown without having to make assumptions about flow pathway geometry. In practice, if a rapid tracer response is obtained after test 1, test 2 should probably be started within a factor of 2 or so of the end of test 1 to reduce the chances of a thermal drawdown occurring before the second test is completed, which would defeat the purpose of the second test. A different thermally-degrading tracer may also be necessary for test 2 if the tracer used in the first test lingers.

## 6. Conclusions

From a practical standpoint, the results and interpretation of the 2017 LDG reactive tracer test have indicated that the time to thermal drawdown at well P as a result of injecting cool/spent water into well I is likely not much more than about 500 days, assuming an injection rate of 500 gpm into well I. If there is a significant amount of porous media flow through the flow pathways, the time to thermal drawdown could be shorter. Thus, the decision to stop using well I as an injection well after the rapid nonreactive tracer response in the 2016 nonreactive tracer test appears to be justified (as long as well P is used as a production well), and it is certainly consistent with conventional reservoir management practices. However, the magnitude of thermal drawdown in well P is estimated to be less than 8ºC over about 5 years if 100ºC water is steadily injected into well I, which is rather minimal (mainly because of the relatively low production temperature of well P). Both the 2016 and the 2017 tracer tests have been used to make informed decisions to manage the geothermal reservoir at LDG in a manner that avoids adverse impacts to the power plant and to other users of the geothermal resource.

## 6. Acknowledgments

The authors are grateful to Cyrq Energy, Inc., and their subsidiary Lightning Dock Geothermal, HI-01 LLC, for providing access to their geothermal plant, for coordinating tracer injection permitting, and for logistical support during the tracer tests. We especially acknowledge Michelle Henrie, Nick Goodman, David Ramirez, Kacie Peterson, and Tara

Shannon for their invaluable support. Kai Williams, George Perkins, and Kate Norskog assisted with tracer analyses and with the elevated-temperature cesium sorption experiments at Los Alamos National Laboratory. This work was partially supported by the Los Alamos National Laboratory New Mexico Small Business Assistance Program. The remainder of the support was from the U.S. Department of Energy, Office of Energy Efficiency and Renewable Energy, Geothermal Technologies Office. Los Alamos National Laboratory is operated by Los Alamos National Security, LLC, for the National Nuclear Security Administration of the U.S. Department of Energy (Contract DEAC52-06NA25396).

## 7. References

Dean, C.A., Reimus, P., Oates, J, Rose, P, Newell, D., and Petty, S. 2015. Laboratory experiments to characterize cation-exchanging tracer behavior for fracture surface area estimation at Newberry Crater, OR. *Geothermics*, 53, 213-224.

Elias, G., E.D. Mattson, and J.E. Little. 2012. A HPLC method for the quantification of butyramide and acetamide at ppb levels in hydrogeothermal waters, *Anal. Methods*, 4, 530-533.

Elston, W.E., E.G. Deal, and M.J. Logsdon. 1983. Geology and geothermal waters of Lightning Dock region, Animas Valley and Pyramid Mountains, Hidalgo County, New Mexico, *Circular 177*, New Mexico Bureau of Mines and Mineral Resources, Socorro, NM.

Fisher, J.R. and H.L. Barnes. 1972. Ion-product constant of water to 350 deg., *J. Phys. Chem.*, 76, 431-448

Lawton, T. F, and R.E. Clemons. 1992. Klondike basin-late Laramide depocenter in southern New Mexico, *New Mexico Geology*, 14, p. l-7.

Lawton, T. F. 2000. Inversion of Late Jurassic-Early Cretaceous extensional faults of the Bisbee Basin, southeastern Arizona and southwestern New Mexico, *N. M. Geological Society, 51st Field Conference Guidebook,* p. 95- 102.

Lenhardt, N., and Gotz, A.E. 2015. Geothermal reservoir potential of volcaniclastic settings: The Valley of Mexico, Central Mexico, *Renewable Energy*, 77, 423-429.

Reimus, P.W., Pohll, G., Mihevc, T., Chapman, J., Papelis, L., Lyles, B., Kosinski, S., Niswonger, R., Sanders, P. 2003. Testing and parameterizing aconceptual model for radionuclide transport in a fractured granite using multiple tracers in a forced-gradient test. *Water Resour. Res.*, 39 (12), 1350, http://dx.doi.org/10.1029/2002WR001597.

Reimus, P., Marina, O., Norskog, K., Caporuscio, F., Perkins, G., and Sams, S. 2016. Results and interpretation of a 2016 tracer test at the Lightning Dock Geothermal Facility and planning for a reactive tracer test in 2017. Confidential New Mexico Small Business Assistance report provided to participating companies, Los Alamos National Laboratory, Los Alamos, NM.

Reimus, P., Dean, C. and Newell, D. 2018. Evaluation of a cation-exchanging tracer to interrogate fracture surface area in enhanced geothermal systems. *Geothermics*, 71, 12-23.

Robinson, B.A. and J.W. Tester. 1990. Kinetics of alkaline hydrolysis of organic esters and amides in neutrally-buffered solution, *Int. J. Chem. Kinetics*, 22, 431-448.

Rose, P.E., W.R. Benoit, and P.M. Kilbourn. 2001. The application of polyaromatic sulfonates as tracers in geothermal reservoirs, *Geothermics*, 30, 617-640.

Williams, M.D., P.W. Reimus, V. R. Vermeul, P.E. Rose, C.A. Dean, T.B. Watson, D.L. Newell, K.B. Leecaster, and E.M. Brauser. 2013. Development of Models to Simulate Tracer Tests for Characterization of Enhanced Geothermal Systems, *PNNL-22486*, Pacific Northwest National Laboratory, Richmond, WA.

Witcher, J.C. 2008. Evidence for a large-scale Laramide tectonic inversion and a mid-Tertiary caldera ring fracture zone at the Lightning Dock geothermal system, New Mexico, *New Mexico Geological Society Guidebook, 59th Field Conference, Geology of the Gila Wilderness-Silver City Area*, p. 177-188.